The Structure of Highly Dispersed SiO_2-Supported Molybdenum Oxide Catalysts during Sulfidation

M. de Boer,* A. J. van Dillen, D. C. Koningsberger, and J. W. Geus

Department of Inorganic Chemistry, University of Utrecht, P.O. Box 80083, 3508 TB Utrecht, The Netherlands

Received: January 31, 1994; In Final Form: May 20, 1994®

The structure of sulfided Mo-catalysts and their oxidic precursors has been abundantly studied, but the genesis of the active phase has remained much less investigated. The sulfidation (in H_2S/H_2 atmosphere) of a series of MoO_3/SiO_2 catalysts has been examined by means of temperature-programmed sulfidation, X-ray absorption fine structure, and transmission electron microscopy. The oxidic, oligomeric clusters in a 5.6 wt % MoO_3/SiO_2 catalyst are transformed into partly sulfided particles (MoO_xS_y) by O—S exchange at room temperature. A molybdenum sulfide species the structure of which resembles the MoS_3 structure is formed during sulfidation at 423 K. The MoS_2 phase is formed at temperatures between 523 and 573 K, depending on the dispersion of the initial MoO_3 phase. The transition of MoS_3 into MoS_2 can be monitored by the evolution of H_2S from the catalyst with a simultaneous consumption of H_2. The two-dimensional size of the MoS_2 slabs can be derived from the EXAFS Mo—Mo coordination number by means of a theoretical model. TEM is required to elucidate the stacking height of the slabs.

1. Introduction

The application of supported molybdena-based catalysts in industrial processes, such as partial oxidation[1-5] and hydrotreating,[6-18] has rendered supported molybdenum oxide catalysts a main subject of investigations. Many studies are dedicated to the preparation and the structure of MoO_3 catalysts on different supports. The *sulfided* counterpart of the *oxidic* precursors of Co(Ni)/Mo(W) catalysts is one of the most thoroughly investigated catalyst systems. Conversion of the oxidic catalyst into the active sulfide occurs under reaction conditions, due to presulfiding or the presence of sulfur-containing feedstocks. It is industrial practice to "spike" the feedstock with agents, such as CS_2, dimethyl sulfide (DMS), or dimethyl disulfide (DMDS), to accelerate the sulfidation of the catalyst.[19,20] As an alternative, the catalyst can be sulfided *ex situ* by impregnation with a sulfur-containing liquid. *In situ* heating of the catalyst subsequently leads to sulfidation.[21] In most of the laboratory tests the catalyst is sulfided by a mixture of H_2S/H_2 at high temperature[22,23] or in a temperature program.

A number of models have been proposed to explain the activity of the Co(Ni)/Mo(W) catalysts. Consensus exists on the structure of the molybdenum sulfide phase: under typical hydrotreating conditions (*i.e.*, p = 10–200 bar, T = 573–723 K, excess H_2, and a sulfur-rich feedstock[13]) MoS_2 is present, in which molybdenum is trigonal prismatically coordinated by sulfur atoms.[24-33] However, the position and the role of the cobalt atoms in the catalysts are still debated. The earlier proposed models are based on the assumption of a *monolayer*,[34] *contact synergy*,[15,18] *intercalation*,[35,36] and *remote control*.[37]

The most popular model is based on publications by Topsøe *et al.*[30] and by Wivel *et al.*[38] The latter reported a linear relationship between the activity in thiophene HDS and the concentration of Co present in the "Co—Mo—S" species. This phase had been designated as "CoMoS"[30] because its Mössbauer spectrum did not resemble any of the known cobalt sulfide or cobalt molybdenum sulfide spectra. The CoMoS species is envisioned as a MoS_2 layer (*slab*), with cobalt atoms decorating the edges.[30,39] Since the introduction of this model, some important publications have made it questionable. Perhaps the most striking fact is that a set of alternatively prepared catalysts (van Veen *et al.*[40]) with identical Mössbauer fingerprints exhibited a different activity in thiophene HDS. Moreover, a carbon-supported Co catalyst (without Mo) appears to have the same Mössbauer spectrum as the "CoMoS" spectrum.[41,42] The observations with the carbon-supported catalyst can be explained by assuming that highly dispersed cobalt sulfide clusters are the active species for HDS.[41,43-46]

The nature of the active sites and the mechanism of the HDS reaction have received much attention, but the genesis of the active phase has remained relatively scarcely studied. Publications of Payen,[26] Pratt,[27] and Knözinger provide valuable information about the sulfidation of MoO_3 catalysts. Systematic research by several co-workers of Moulijn[47-50] has most significantly contributed to the understanding of the sulfidation of HDS catalysts. The use of temperature-programmed sulfidation (TPS) techniques yields useful information on the sulfidation process, but it is difficult to extract information about the structure of the intermediate species during sulfidation. Therefore, other *in situ* techniques, such as LRS,[13,26,51] Mössbauer spectroscopy,[9,22,38,41,42,46,52] and XAFS[33,53-60] are needed. The formation of MoS_2 slabs can be elegantly monitored by (high resolution) TEM.[7,8,26-28,48,61-65] Direct preparation of a sulfidic structure (instead of sulfidation of a previously prepared oxidic catalyst) can be accomplished with the so-called *HSP method*, in which a (cobalt-)molybdenum sulfide is precipitated from homogeneous solution in the absence or presence of a support.[29,30,66-68] Another method is the thermal decomposition of $(NH_4)_2MoS_4$ (ATM), often referred to as the *impregnated thiosalt preparation* (ITP).[29,68-70] Application of other molybdenum- and sulfur-containing complexes may lead to improved control of the structure of the catalyst.[71,74]

The majority of the literature in this field is dedicated to alumina-supported catalysts, because highly dispersed alumina-supported Co–Mo catalysts can easily be prepared on laboratory and industrial scales. A drawback of Al_2O_3 as a support is its tendency to form spinels with Co and Ni[72,73] that possess low activity in hydrotreating reactions, and its poor resistance toward acid gases such as SO_2. SiO_2 does not suffer from the latter disadvantage, but it is known to form cobalt and nickel(hydro)-silicates.[75]

In this paper a well-defined MoO_3/SiO_2 catalyst[76] will be used

* To whom correspondence should be addressed at Akzo Nobel Chemicals B.V., Nieuwendammerkade 1-3, P.O. Box 37650, 1030 BE Amsterdam, The Netherlands.

® Abstract published in *Advance ACS Abstracts*, July 1, 1994.

0022-3654/94/2098-7862$04.50/0

TABLE 1: Sulfidation Procedure of the 5.6 wt % MoO_3/SiO_2 Catalyst for the Application of TEM and *in Situ* XAFS

no.	code	sulfidation procedure
1	Mo6-RT	flush Ar; H_2S/H_2/Ar; 30 min at room temperature (295 K)
2	Mo6-423	as 1; ramp to 423 K (5.0 K min^{-1}); 30 min at 423 K; ramp to RT (5.0 K min^{-1}); flush Ar
3	Mo6-673	as 1; ramp to 673 K (5.0 K min^{-1}); 30 min at 673 K; ramp to RT (5.0 K min^{-1}); flush Ar

for a study of the sulfidation behavior. The process of sulfidation can be easily monitored using TPS by measuring the concentrations of both H_2S and H_2. The sulfur content of the catalyst at different sulfidation temperatures can be established with temperature-programmed oxidation, using the area under the SO_2-evolution peak. After determination of the sulfidation as a function of the temperature, the transformation of the oxide into a sulfide will be investigated at intermediate temperatures by means of *in situ* techniques, such as XAFS and *ex situ* TEM.

2. Experimental Section

Preparation. The catalysts used in this paper have been described elsewhere.[76] The codes are related to the MoO_3 loading: Mo6, Mo11, and Mo26 denote 5.6, 11.3, and 26.0 wt % MoO_3 on SiO_2, respectively. The SiO_2-supported MoO_3 catalysts were prepared by deposition precipitation of trivalent molybdenum (Mo^{3+}, prepared electrochemically in HCl) from homogeneous solution onto SiO_2 (Degussa, Aerosil 200V, BET S.A.: 186 m^2/g). The deposition was brought about by raising the pH of a suspension of SiO_2 in a diluted Mo^{3+} solution. The pH was raised by decomposition of urea at 363 K. The suspension was filtrated when the pH reached a value of 7. The filtrate was washed with demineralized water and dried in air at 393 K for 16 h. Subsequently, the catalysts were calcined in air at 723 K for 16 h. The catalysts were white after calcination and turned blue after hydration under ambient conditions.[76]

Characterization. *Temperature-Programmed Sulfidation.* Temperature-programmed sulfidation (TPS) profiles are recorded in an automated microflow apparatus. The apparatus consists of a gas flow dosing system, a quartz reactor (i.d.: 8 mm), and a combination of a thermal conductivity detector (TCD) (Beckmann) and a UV/vis detector (Varian). Gas analysis is executed by sequentially leading the gas stream prior to and behind the reactor through both detectors. Quartz cuvets (Hellma, 20 mm) are used for the UV/vis analysis. H_2S is detected at $\lambda = 232$ nm. The TCD measures the H_2 concentration.

The standard sulfidation comprises the following procedure: sulfidation of 200 mg of catalyst (pelleted at 100 MPa and crushed to a sieve fraction of 425–625 μm) in a 100 mL min^{-1} flow of H_2S/H_2/Ar (10/40/50). After the entire system is flushed, the catalyst is sulfided at room temperature (295 K) for 30 min (isothermal stage). Subsequently, the temperature program is started (5.0 K min^{-1}). At the final temperature, the catalyst is exposed to the same gas flow for another 30 min; subsequently, the sample is cooled to room temperature under the same conditions (vide Table 1). In this paper we use a code indicating the final sulfidation temperature; viz., Mo6-423 means catalyst Mo6 sulfided according to the above mentioned procedure at a final temperature of 423 K.

Temperature-Programmed Oxidation. Temperature-programmed oxidation (TPO) is executed in a 100 mL min^{-1} flow of O_2/Ar (10/90). After the system is flushed with Ar and comes to equilibration at room temperature, the temperature program is started (5.0 K min^{-1}). At the final temperature of 773 K the sample is cooled in O_2/Ar. The sulfur content in the sample is determined from the area under the SO_2 evolution curve, after calibration. SO_2 is measured at its absorption peak at $\lambda = 285$ nm.

The TPS profiles give an overall impression of the sulfidation process, whereas transmission electron microscopy (TEM) and spectroscopic techniques (XAFS) are intended to make "snapshots" of the structure of the catalysts at different, well-defined stages of the sulfidation.

XAFS. The X-ray absorption spectra are recorded at EXAFS station 9.2 of the S.R.S. at Daresbury, U.K. The energy range measured lies between 19 900 and 20 800 eV. The Mo K-edge for Mo-foil is positioned at 19 999 eV. The station is operated with a double-crystal monochromator, Si(220), detuned to 50% intensity to minimize the presence of higher harmonics in the beam. The measurements are carried out in transmission mode with optimized ionization chambers to measure the intensity before and behind the sample. Data are collected at each energy for 1 s, and results from 6 scans are averaged to minimize high- and low-frequency noise. The samples are pressed into self-supporting wafers (each with an absorbance of approximately 2.5) and mounted in an *in situ* EXAFS cell.[90] The spectra are recorded under a helium atmosphere at 77 K.

Standard procedures are used to extract the XAFS data from the measured absorption spectra. The energy range used for the isolation of $\chi(k)$ is generally about $\Delta k = 3.5$–13 Å; the exact values are given for each plot separately in the captions of the figures. Normalization is done by dividing the absorption intensities by the height of the absorption edge and subtracting the background by using cubic spline routines.[91] The final EXAFS function is obtained by averaging the individual background-subtracted and normalized EXAFS data. A statistical error per data point is calculated for the averaged EXAFS function. The data analysis is performed on an isolated part of the data obtained by an inverse Fourier transformation over a selected range in R-space.[91] Averaging the individually Fourier-filtered EXAFS data yields the statistical errors per data point in the isolated EXAFS functions. The statistical error in the data points can be used to calculate the statistical error in the fit parameters (ΔN, $\Delta\Delta\sigma^2$, ΔR, and ΔE°). The statistical error does not include systematic errors. Experimental references are used for the data analysis: Na_2MoO_4 for the Mo–O, and MoS_2 for the Mo–Mo contribution. Details of the references are described elsewhere.[76,92]

3. Results and Discussion

The structure of the catalyst Mo6 in oxidic form has been extensively studied. Under ambient conditions the structure of the molybdena phase can be described as hydrated, oligomeric clusters of molybdenum oxide, usually denoted as polymolybdate in MoO_3/Al_2O_3 catalysts. The structure of the (hydrated) clusters under ambient conditions resembles that of heptamolybdate in aqueous solutions ($Mo_7O_{24}^{6-}$). Under dehydrated conditions (after thermal treatment of the catalyst at temperatures above 450 K) the structure of the molybdenum oxide clusters changes.[76] Although MoO_3/SiO_2 catalysts are usually less disperse than MoO_3/Al_2O_3 (lower affinity of Mo^{6+} for SiO_2 than for Al_2O_3[5,93,94]), Mo6 possesses a high dispersion due to the preparation procedure; the interaction between Mo^{3+} and SiO_2 ensures a better dispersion.[76,93,94] Due to its uniformity and the well-known structure of Mo6, this sample has been chosen to study the sulfidation process.[93]

3.1. Sulfidation of MoO_3 Catalysts. *Survey of the Literature.* Arnoldy[47] reports on the sulfidability of *bulk* MoO_3 with H_2S. According to this author, sulfidation proceeds during a TPS experiment via the unstable MoO_2S, that subsequently reacts to form MoO_2 and elemental sulfur. Formation of MoS_2 would proceed by reaction of the MoO_2 with H_2S or by intermediate formation of zerovalent Mo (reduction by H_2) and subsequent reaction of the metal with H_2S under release of hydrogen. Reduction of MoO_3 by H_2S is much faster than reduction by H_2, because the exchange of oxygen for sulfur is easier than the breakage of a Mo—O bond as needed in the reduction of MoO_3

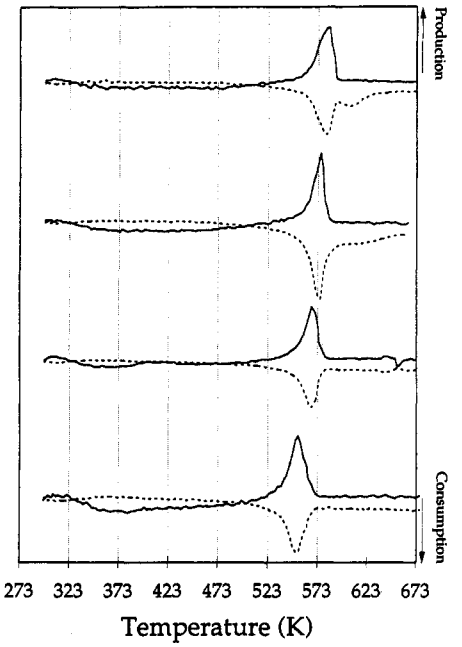

Figure 1. TPS profiles of (from the bottom) Mo6, Mo11, Mo26, and bulk MoO_3. The solid curve is [H_2S], spectrophotometrically measured at 232 nm, and the dashed curve is the HWD signal, predominantly representing [H_2]; ↑ indicates H_2S (H_2) production, and ↓ indicates H_2S (H_2) consumption.

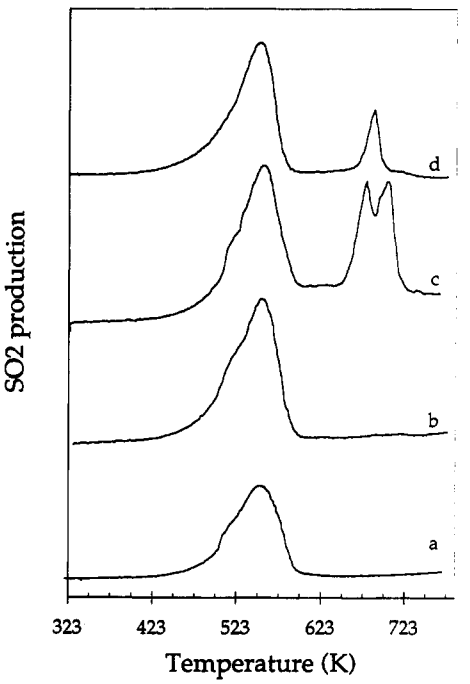

Figure 2. TPO profiles of (a) Mo6, (b) Mo11, (c) Mo26, and (d) bulk MoO_3. The curve indicates the concentration of SO_2 in the effluent gas, spectrophotometrically measured at 285 nm.

with H_2. Water, the reaction product of reduction by H_2, hinders the reduction because it poisons the sites for H_2 dissociation on MoO_3.

The reaction scheme via MoO_2S and MoO_2 proposed for bulk MoO_3 is unlikely for supported MoO_3 catalysts. Several other authors[19,26,33,42,47,51,77] report on the low-temperature sulfidation of supported catalysts. Arnoldy suggests that elemental sulfur is formed during the sulfidation of supported MoO_3 catalysts at low temperature, implying a reduction of Mo^{6+} by sulfide ions.

Partial exchange of oxygen by sulfur may lead to oxysulfide species, $Mo^{VI}O_{4-x}S_x^{2-}$ or $Mo^{VI}O_{3-x}S_x$. These species are well known in aqueous solutions[47,70,78] and can be prepared by adjusting the O/S ratio of a solution of MoO_4^{2-} through addition of $(NH_4)_2S$ or MoS_4^{2-}. Full exchange of oxygen for sulfur atoms would result in MoS_3. Some publications are known in the literature concerning this amorphous compound.[26,47,51,70,79-81,84,85] It can be prepared by acidifying an aqueous ammonium thiomolybdate (ATM) solution, or by gentle decomposition of ATM in vacuo at 473 K.[70] It is implicitly assumed that the valence of molybdenum remains 6+ during the oxygen–sulfur exchange. The valence of molybdenum in MoS_3 is, however, 5+, due to an internal redox reaction between molybdenum and its sulfur ligands ($Mo^{VI} \rightarrow Mo^{V}$ and $2S^{2-} \rightarrow S_2^{2-}$). The resulting *molybdenum–sulfido* complex can be denoted as $[Mo_2^{V}S^{II}_4(S_2^{I})_2]^{2-}$, $[Mo_2^{V}(S_2^{I})_6]^{2-}$, or $[Mo_2^{V}S_8^{I,II}]^{2-}$.[26,47,84,85]

The unstable MoS_3 can easily decompose into MoS_2 and S (or MoS_2 at H_2S in the presence of H_2). Moist ATM decomposes under N_2 at 527 K (dry ATM at 628 K), while MoS_3 decomposes between 513 and 673 K. The decomposition in an inert atmosphere is endothermic (volatilization of sulfur) at low temperature, followed by an exothermic effect due to crystallization of MoS_2.[70] The release of an excess of sulfur is manifested in a TPS profile by the H_2S evolution peak, coinciding with H_2 consumption.

Results. The TPS profiles of Mo6, 11, 26, and bulk MoO_3 are presented in Figure 1. The consumption/production of both H_2S and H_2 is given. After the equilibration of the system in $H_2S/H_2/Ar$ at room temperature, some H_2S evolves at the start of the temperature program, probably due to release of physisorbed H_2S.[47] Subsequently, H_2S absorption proceeds up to a temperature of about 530 K, depending on the MoO_3 loading. The catalysts sulfided at room temperature (Mo6-RT) and at 423 K (Mo6-423) are brownish, whereas sulfidation at temperatures beyond the H_2S evolution peak in TPS leads to black samples. The color of MoS_3 and several intermediate molybdenum oxysulfides is brown, in contrast to the black color of MoS_2.[26,47,70]

Since no H_2 consumption is observed in the low-temperature range of the TPS, it is assumed that exchange between lattice oxygen and sulfur from H_2S takes place, according to eq 1:

$$MoO_3 + xH_2S \rightarrow MoO_{3-x}S_x + xH_2O \qquad (1)$$

The extent of oxygen–sulfur exchange, *i.e.*, the value of x, is hard to quantify from the TPS profiles. At higher temperature, H_2S evolves in a sharp peak, accompanied by H_2 consumption. Obviously, the sample is reduced at this temperature (H_2 consumption) with simultaneous release of H_2S. From the color of the samples Mo6-423 and Mo6-673 and the properties of MoS_3 (vide supra), it is likely that a MoS_3-like species is transformed into MoS_2 (eq 2).

$$MoS_3 + H_2 \rightarrow MoS_2 + H_2S \qquad (2)$$

The peak positions corresponding to the evolution of H_2S are positioned at temperatures increasing in the sequence Mo6, Mo11, Mo26, and bulk MoO_3. The increasing temperature is attributed to the size, *i.e.*, reactivity, of the MoO_3 clusters in the catalysts. The small clusters in Mo6 can be easily sulfided and more readily release the excess of sulfur (reaction 2) than do large particles (as in Mo26, bulk MoO_3), in which a more severe lattice reconstruction is required. At temperatures beyond the H_2S evolution peak some additional H_2S is taken up.

3.2. Temperature-Programmed Oxidation (TPO). The sulfided catalysts are reoxidized by O_2 in a TPO experiment. The total amount of SO_2 set free is a good measure of the sulfur content of the sample. Relatively few authors have applied the TPO technique to sulfide catalysts, although it is very helpful to quantify the sulfur species in solid samples, as dealt with by van Doorn[83] and Yoshimura.[82]

TPO profiles of the MoO_3/SiO_2 catalysts and bulk MoO_3 are presented in Figure 2. The position of the peaks in TPO varies

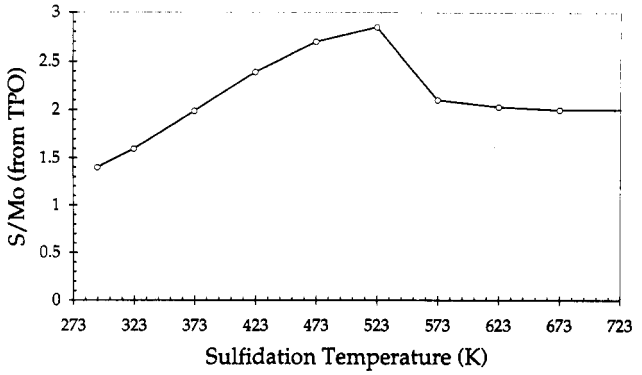

Figure 3. S/Mo ratio, determined by TPO, at different final sulfidation temperatures of catalyst Mo6.

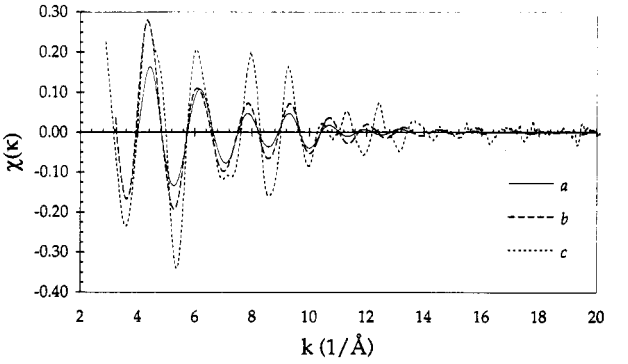

Figure 4. $\chi(k)$ of (a) Mo6-RT, (b) Mo6-423, and (c) Mo6-673 (see Table 1).

in the series. The most highly dispersed sample (Mo6) has the lowest onset temperature for the reoxidation; this sample also has the lowest reduction temperature (vide supra). Bulk MoO_3 and Mo26 exhibit a second peak at higher temperatures. Mo26 even shows a double, fairly large peak at about 673 K. The thermal effects during reoxidation of the sulfided catalysts are considerable. The S/Mo ratio at intermediate stages of the sulfidation can be established by means of TPO. The S/Mo ratio as a function of the sulfidation temperature is plotted in Figure 3. The measurements are accomplished by TPO experiments after sulfidation of fresh Mo6 (Table 1) until various final temperatures. Figure 3 shows that S/Mo = 1.4 after sulfidation at 295 K (RT), indicating a $MoO_{1.6}S_{1.4}$ stoichiometry of the clusters when only O–S exchange takes place. This suggests a sulfidation degree of almost 50% at room temperature. Since supported MoO_3 catalysts are very reactive toward H_2O, it is fair to assume that H_2S also reacts with the molybdenum oxide clusters at this temperature. Figure 3 also reveals that the S/Mo ratio amply exceeds the value for MoS_2 at temperatures below the reduction peak in TPS. Beyond the reduction temperature the MoS_2 stoichiometry (S/Mo = 2) is found.

3.3. X-ray Absorption Fine Structure (XAFS). The structure of the molybdenum–(oxy)sulfide phase in Mo6 during the sulfidation process will be investigated using XAFS. The raw $\chi(k)$ data of Mo6-RT, Mo6-423, and Mo6-673 are shown in Figure 4a–c. The $\chi(k)$ curves of the sulfided samples are the average of four separately isolated $\chi(k)$'s. The same applies to isolated EXAFS curves (Fourier-filtered) that are used for data analysis. The k^1-weighed FT's and the best fits on Mo6-RT, Mo6-423, and Mo6-673 are shown in Figure 5a–c. The corresponding fit parameters are listed in Table 2.

Analysis of the Structure after Sulfidation at 295 K (RT). The FT of the fit on Mo6-RT (Figure 5a) and the corresponding parameters in Table 2 suggest a high level of sulfidation of the cluster at room temperature. The coordination number for Mo—S (N_{Mo-S}) amounts to 4.83, whereas the number of oxygen atoms around the molybdenum atom is only 0.17. The small statistical error in N_{Mo-O} (ΔN) indicates that this modest contribution is no oddity or "fit-artifact" (vide infra). From this data, an extent of sulfidation of about 0.97 $(1 - 0.17/(0.17 + 4.83))$ is suggested. The extent of sulfidation could be defined as the number of sulfur neighbors as determined by EXAFS divided by the total number of neighbors in the first shell. The extent of sulfidation as derived from EXAFS (*i.e.* 97%) is much higher than that derived from TPO experiments (vide supra). TPO is probably a more reliable tool to determine the overall sulfur content, because EXAFS

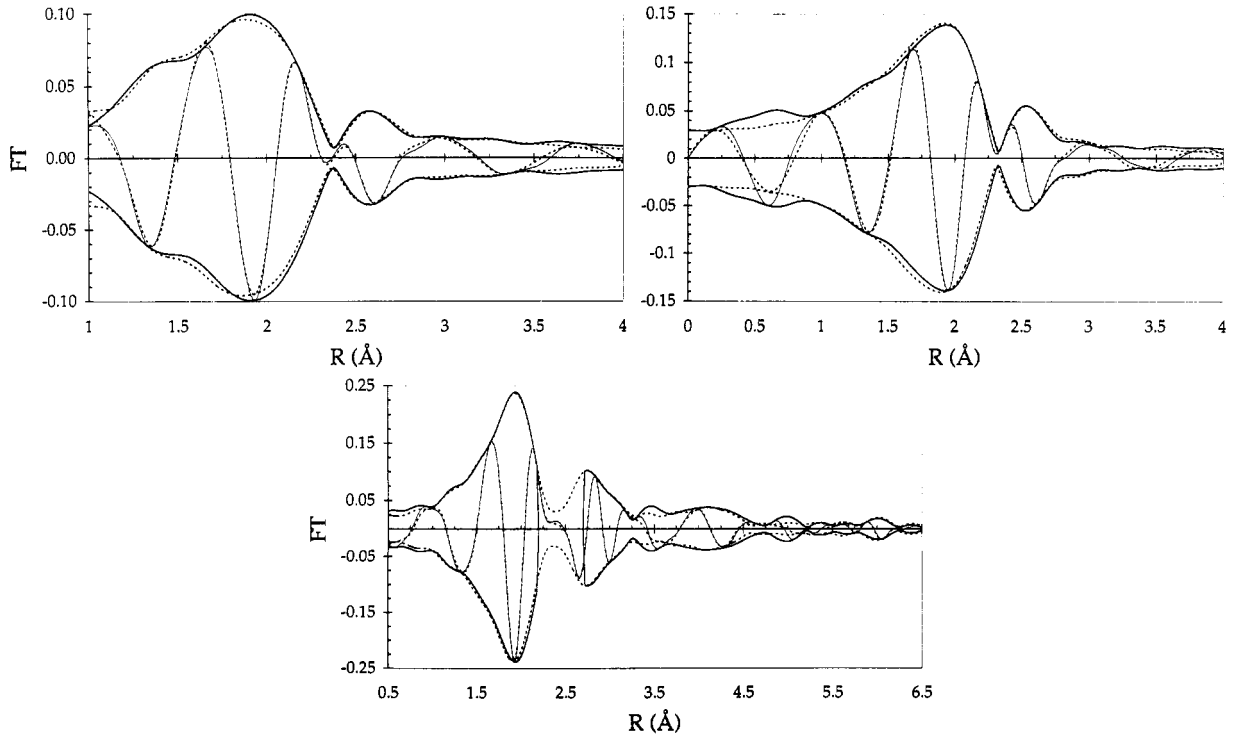

Figure 5. Magnitude (envelope) and imaginary part (oscillations within the envelope) of the k^2-weighted FT of the isolated $\chi(k)$ (solid curve) and fit (dashed curve) of (a) Mo6-RT (Δk = 3.70–12.84 Å^{-1}), (b) Mo6-423 (Δk = 3.70–13.72 Å^{-1}), and (c) Mo6-673 (Δk = 3.70–12.83 Å^{-1}).

TABLE 2: Fit Parameters of the Analysis of Mo6-RT, Mo6-423, and Mo6-673

scatterer	N	ΔN	$\Delta\sigma^2$ (10^{-4} Å^2)	$\Delta\Delta\sigma^2$ (10^{-4} Å^2)	R (Å)	ΔR (Å)	E_0 (eV)	ΔE_0 (eV)
Mo6-RT N_{fit} = 16, $N_{allowed}$ = 31.6								
O	0.17	0.01	−47.2	4.2	1.666	0.007	−9.95	2.43
S	4.83	0.04	87.0	0.6	2.435	0.001	0.67	0.12
Mo	1.14	0.05	56.7	2.3	2.769	0.001	4.62	0.30
Mo	2.59	0.03	253.7	0.6	3.450	<0.001	0.95	0.09
Mo6-423 N_{fit} = 8, $N_{allowed}$ = 25.4								
S	8.08	0.01	99.8	0.1	2.445	<0.001	1.46	0.05
Mo	1.72	0.02	37.6	0.4	2.755	<0.001	8.76	0.13
Mo6-673 N_{fit} = 16, $N_{allowed}$ = 38.5								
S	6.00	0.03	20.5	0.3	2.407	<0.001	2.86	0.05
Mo	4.68	0.03	33.3	0.3	3.161	<0.001	0.54	0.08
S	8.48	0.13	70.9	1.3	4.733	0.001	0.83	0.13
Mo	2.25	0.18	−30.1	5.7	6.323	0.006	−0.74	0.79

analysis can be disturbed by interference of different scatterers at comparable coordination distances.

It will be shown that a Mo—O and a Mo—S contribution can be distinguished by means of EXAFS analysis. The Mo—S coordination distance of 2.435 (±0.001) Å is slightly higher than the Mo—S distance in MoS_2 (2.41 Å). The length of the remaining Mo—O contribution (1.666 (±0.007) Å) is small and most likely corresponds to a terminal Mo=O bond. The negative value of the Debye–Waller factor for Mo—O in this sample points to a smaller disorder than the reference (Mo—O in Na_2MoO_4), which complies with the short coordination distance and, hence, the strong Mo—O bond. These strongly bonded oxygens apparently are not yet exchanged by sulfur at this temperature. A more striking difference with both the fully oxidic state (MoO_3) and the fully sulfided state (MoS_2) is the Mo—Mo coordination distance of 2.769(±0.001) Å. The value for N_{Mo-Mo} found here (1.14) is significantly lower than that in the oxidic cluster, but a Mo—Mo contribution at 3.450 Å is additionally found.

Distinction between a Mo—S and a Mo—O Scatterer. The existence of the Mo—O coordination can be proven by *difference file technique*: Figure 6a,b presents the fit of a Mo—O and a Mo—S shell on the difference file of the raw data of Mo6-RT *minus* the Mo—S and the Mo—Mo shell (as in Table 2), respectively. The magnitude of the FT of the difference file can be fitted by both scatterers (Figure 6a,b), but the imaginary part fits only in the case of oxygen (Figure 6a) and not in the case of sulfur (Figure 6b). This can be understood by the different value of the phase shift (δ_j) for both scatterers, which amounts to π radians. The maxima in the imaginary part of the FT in Figure 6a are therefore the minima in Figure 6b. Thus, it can be concluded that an oxygen scatterer is present. The incorporation of the Mo—S shell in the fit is analogously justifiable.

Analysis of the Structure after Sulfidation at 423 K. After sulfidation at 423 K (Figure 5b), the structure changes significantly. The Mo—Mo coordination number increases to 1.72(±0.02) at a coordination distance of 2.76 Å, but the Mo—Mo contribution at higher coordination distance (3.45 Å in Mo6-RT) is no longer present. The oxygen neighbor at small coordination distance is absent in this sample. The contribution of the sulfur scatterer has increased to a value of 8.08(±0.01), higher than expected for an octahedrally coordinated molybdenum atom. Apparently, the structure of the sulfided cluster cannot be described simply by substitution of the oxygen atoms by sulfur. Some excess of sulfur may be present. The structure of the clusters can be explained using the MoS_3 structure.[84,85] The Mo—Mo distance in MoS_3 amounts to about 2.8 Å, which approaches the distance of 2.76 Å calculated from our EXAFS data. One-dimensional chains of molybdenum are present in MoS_3, which leads to a maximum N_{Mo-Mo} of 2.0 at about 2.8 Å. In the same structure, each molybdenum atom possesses six sulfur neighbors at approximately 2.4 Å[84] and (at least) two sulfur atoms at greater distance (vide Figure 7). As mentioned before, the molybdenum

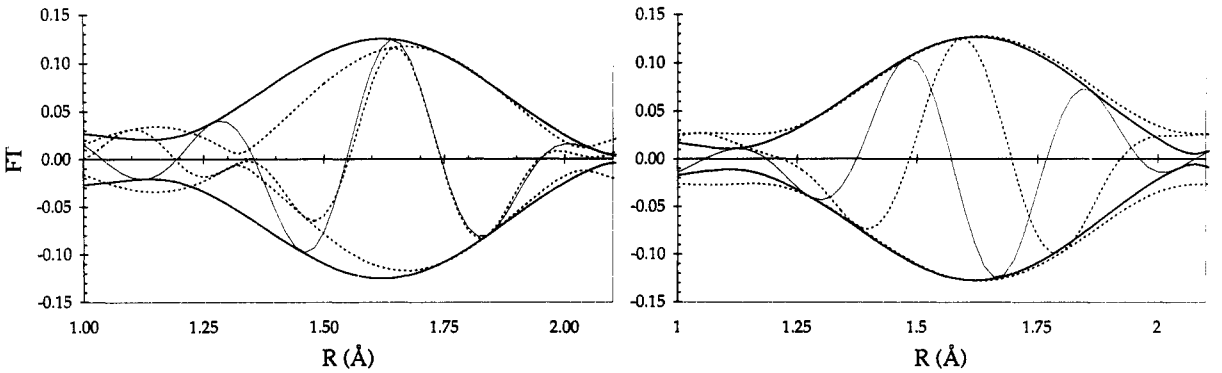

Figure 6. Magnitude (envelope) and imaginary part (oscillations within envelope) of the k^3-weighted FT of the difference file of Mo6-RT (raw *minus* Mo—S and Mo—Mo; Table 2) (solid curve): (a, left) best fit with a Mo—O shell, and (b, right) best fit with a Mo—S shell (fits: dashed).

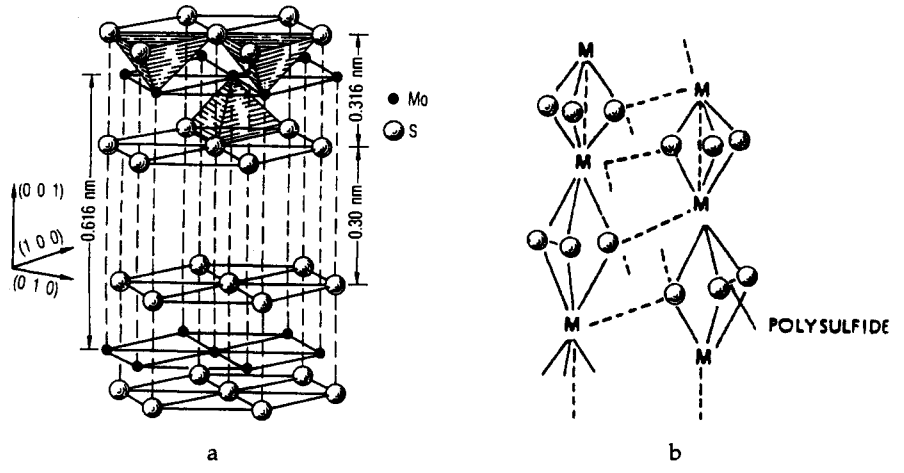

Figure 7. Schematic representation of the structure of (a) MoS_2 (from ref 24) and (b) MoS_3 (slightly adapted from ref 84).

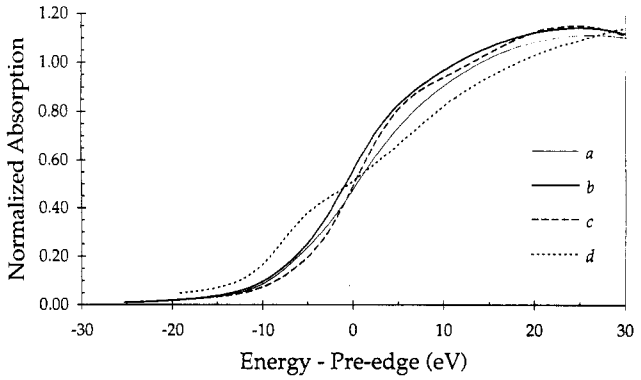

Figure 8. Pre-edges of (a) Mo6-RT, (b) Mo6-423, (c) Mo6-673, and (d) an aqueous solution of 100 mM $(NH_4)_2MoS_4$ (ATM) at pH 10 (assumed tetrahedral coordination).

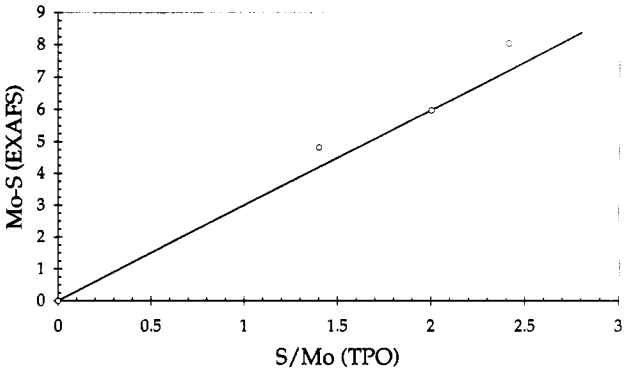

Figure 9. Correlation of the S/Mo ratio with the EXAFS N_{Mo-S}.

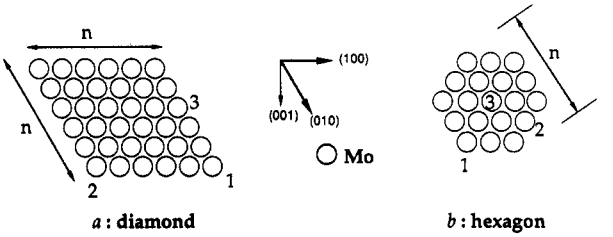

Figure 10. Schematic representation of a two-dimensional plane of hexagonally ordered molybdenum atoms, as in MoS_2 (see Figure 6): (a) diamond model, (b) hexagon. The planes of sulfur atoms have been omitted.

atoms in MoS_3 are pentavalent.[26,84] The S_2^{2-} pairs are indicated in Figure 7. Arnoldy[47] and Mangnus[48] describe this feature by assuming that a nonstoichiometric S_x species is formed that can be reduced with H_2 (a TPR after sulfidation yields a H_2S evolution peak at low temperature).

Analysis of the Structure after Sulfidation at 673 K. The EXAFS analysis of the structure after sulfidation at 673 K is unambiguous (Figure 5c). The coordination distances of Mo—S and Mo—Mo at 2.407(±0.0005) Å and 3.16(±0.0005) Å, respectively, are equal to the distances in MoS_2. The moderate values for the *Debye–Waller factor* ($\Delta\sigma^2$) indicate a rather well-ordered system, but naturally of a higher disorder than the reference compound (bulk MoS_2), because the MoS_2 slabs within Mo6-673 possess a limited particle size. The Mo—S coordination number ($N = 6.00$) is in proper agreement with the value in bulk MoS_2 (6.00), in which molybdenum atoms are trigonal prismatically surrounded by sulfur atoms. The statistical significance of the contributions at higher coordination distances is less good. The contribution of the Mo—Mo scatterer at 6.323 Å (twice the 3.16 Å distance) is probably obscured by multiple scattering effects.[33]

Obviously, an important transformation has taken place between 423 and 673 K. It must be remembered that the reduction of the catalyst (H_2S release and simultaneous H_2 consumption) takes place at about 535 K (Figure 1). The structure of MoS_3 (bulk version of the structure of the cluster intermediately formed) and MoS_2 (bulk version of the final structure) are represented in Figure 7.

Information Derived from the Pre-Edge Structure. The valence of molybdenum changes during sulfidation. Unequivocally, molybdenum is initially present as a hexavalent ion in oxidic form and tetravalent in its final sulfidic state. At intermediate stages, however, the valence is unknown. XPS may be used to assess the valency, but XANES is also valuable in an indirect way. In Figure 8 the pre-edges of Mo6-RT, Mo6-423, Mo6-673, and aqueous MoS_4^{2-} are presented.

The distinct pre-edge peak in curve *d* of $(NH_4)_2MoS_4$ (Figure 8) is due to the 1s → 4d transition in the tetrahedrally coordinated Mo^{6+} cation (comparable to Na_2MoO_4 (T_d)). A tetrahedron is the only stable configuration for *hexavalent* molybdenum–sulfur compounds (this does not apply to oxides). Because the Mo^{4+}: $4d^2$ configuration in the sixfold coordination in MoS_2 lies at the top of the S^{2-}:$3p^6$ band, it must be expected that any octahedrally coordinated Mo^{6+}:$4d^0$ configuration in a sulfide will result in an internal redox reaction, ending up with Mo^{5+} and $(S_2)^{2-}$.[84] The pre-edges of Mo6-RT, Mo6-423, and Mo6-673 do not reveal a pre-edge peak. This implies that no tetrahedral coordination is present in the catalysts. From the above theory it must be concluded that molybdenum cannot be present as Mo^{6+} under these circumstances, meaning that sample Mo6 is reduced to Mo^{5+} by H_2S at room temperature. Further reduction takes place at about 553 K, where the transition of Mo^{5+} to Mo^{4+} takes place.

Calculation of the Lateral Slab Size from EXAFS Data. The value for N_{Mo-S} probes the local environment of the molybdenum atom, but it is questionable whether it represents the S/Mo ratio (see section 3.2). From the observed values for N_{Mo-S} in Mo6-RT, Mo6-423, and Mo6-673, only the S/Mo ratio in Mo6-673 is useful because the structure in Mo6-673 is unambiguous: the N_{Mo-S} of 6.0 in Mo6-673 corresponds to an S/Mo ratio of 2 (MoS_2). Figure 3 in combination with the N_{Mo-S} values acquired from EXAFS analysis can be used to construct a TPO-EXAFS calibration plot (Figure 9). The S/Mo ratio shows a reasonable correlation with the Mo—S coordination number.

While the molybdenum–sulfur coordination probes the average first shell around the molybdenum atom, the N_{Mo-Mo} is a direct measure of the size of the particle. In the case of Mo6-673, the structure of the particle is precisely known, since it duplicates R_{Mo-S} and R_{Mo-Mo} of MoS_2 (bulk). Thus, with the assumption of the MoS_2 structure (Figure 7a), N_{Mo-Mo} can be utilized to estimate the size of the MoS_2 slabs. Because of the simple two-dimensional structure of MoS_2, N_{Mo-Mo} is a good measure of the lateral slab size. If a two-dimensional layer (size $n \times n$) of hexagonally ordered molybdenum atoms is assumed, as in a MoS_2, four different positions can be distinguished (Figure 10a).

The distance between the molybdenum atoms is 3.16 Å. A simple formula for the theoretical value of the coordination number N (N_{model}) as a function of the size of the slab can be derived. Position **1** (Figure 10a) has only two adjacent Mo atoms at 3.16 Å, position **2** has three neighbors, and position **3** and **4** possess four and six adjacent Mo atoms, respectively. The mean coordination number ($N(n)$) can be calculated as a function of the size of the two-dimensional plane (n^2 atoms). The number of Mo atoms in position j ($\#j$) is two for $j = 1$, two for $j = 2$, $4(n-2)$ for $j = 3$, and $(n-2)^2$ for $j = 4$. The formula for the mean Mo—Mo coordination number according to the *diamond model* is given in eq 3. The formula for a *hexagon* (the assumed shape of an MoS_2 slab) is presented in eq 4 without derivation (n is the dimension of the hexagon (cross section); r is a practical parameter that equals $(n-1)/2$, odd values for n give a perfect hexagon).

$$N^{\text{model}}_{\text{Mo—Mo}}(n) = \frac{\sum_{j=1}^{4}(\#_j N_j)}{n^2} = 6 - \frac{8}{n} + \frac{2}{n^2} \qquad (3)$$

$$N^{\text{model}}_{\text{Mo—Mo}}(n(n)) = \frac{24r + 36\sum_{i=1}^{r-1} i}{1 + 6\sum_{i=1}^{r} i} \text{ and } r = \frac{n-1}{2} \qquad (4)$$

This equation is only valid for cases where MoS_2 slabs are present. Thus, only the slab size of sample Mo6-673 can be estimated in this way. The models do not show large differences in the results, except for very small slabs. The value of $N^{\text{model}}_{\text{Mo—Mo}}$ as a function of the size of the model slab (diamond or hexagon) is plotted in Figure 11. Substitution of the experimentally found Mo–Mo coordination number $N^{\text{exp.}}_{\text{Mo—Mo}}$ (*i.e.*, 4.68, vide Table 2) in eq 3 yields a value for n of 5.8. A value of 5.8 corresponds to $n^2 = 34$ molybdenum atoms. According to the hexagon model, this implies a hexagon with a cross section of $n \sim 6$ ($r = 2.5$), which is not a perfect hexagon. Substitution of a large figure for n forces $N^{\text{model}}_{\text{Mo—Mo}}$ to 6, the value for bulk MoS_2 without mentionable contributions of the edge atoms.

The value found for the two-dimensional size of the slabs does not necessarily represent the total MoS_2 slab but may indicate the mean size of MoS_2 subdomains in large, highly stacked MoS_2 slabs.[89] Some authors have questioned the use of the Mo—Mo coordination distance, but for homogeneous samples with small slab sizes, it probably is a good approximation of the average lateral dimension of the slabs. EXAFS probably is the only technique capable of measuring the lateral size of MoS_2 slabs in the level below the detection limits of TEM.

One aspect is neglected in the model for the calculation of the particle size of the MoS_2 crystallites: the MoS_2 phase is usually present as a stack of MoS_2 slabs. The distance between the slabs is 6.16 Å, according to the literature[24,25,27,28,52] and cannot be seen in EXAFS due to multiple scattering effects and interference with $R_{\text{Mo—Mo}}$ at 6.32 Å (twice 3.16 Å) in the two-dimensional plane. Therefore, a complementary technique is required to investigate the height of the MoS_2 stacks.

Transmission Electron Microscopy for Stack Height Evaluation. TEM is very appropriate to investigate the stacking of the MoS_2 slabs.[7,26–28,31,48,61–65] A TEM micrograph of Mo6-673 is shown in Figure 12. The stacks of MoS_2 slabs can be easily distinguished. Obviously, some variation in the stack height exists. The mean stack height amounts to about 3. We have to bear in mind that some (probably unstacked) slabs may be present that are too small to be detected by TEM. Examination of Mo6-423 reveals that no slabs are present after sulfidation at 423 K. For this reason the micrograph has been omitted.

Earlier results[76] have demonstrated that the structure of the cluster in Mo6 alters drastically upon thermal treatment: it disintegrates and spreads over the support due to the removal of stabilizing hydroxyl groups in the molybdenum (hydr)oxide cluster. EXAFS analysis (not presented) demonstrates that sulfidation at 673 K of a thermally pretreated Mo6 leads to the same structure as Mo6-673 (without thermal pretreatment). Apparently, the structure of sulfided Mo6 does not depend on the path followed during sulfidation. The rebuilding of the "spreaded" Mo6 occurs under sulfiding conditions, which annihilates the impact of a preceding thermal treatment.

4. Concluding Remarks

An *in situ* study of the structure of a MoO_3 catalyst during sulfidation can be successful only when the initial structure of the oxidic phase is very well-known. A series of MoO_3/SiO_2 catalysts of increasing MoO_3 loading is helpful to examine trends in the sulfidation behavior with techniques such as TPS. It appears that sulfidation proceeds roughly by H_2S uptake until low temperatures (below 523 K), which transforms the catalyst into a brownish MoS_3-like structure. Subsequently, the unstable MoS_3-like structure is reduced to MoS_2 under the influence of H_2. The related H_2S evolution is well noticeable in a TPS pattern and characterizes the dispersion of a catalyst. In the series of MoO_3/SiO_2 catalysts, this peak shifts from 553 K for Mo6, via 565 K (Mo11), and 578 K (Mo26) to 585 K for bulk MoO_3 (physically mixed with SiO_2). The most highly dispersed MoO_3 catalyst, *i.e.*, Mo6, is completely converted into the MoS_3-like structure at 473 K. MoS_3 is even known to decompose within an inert atmosphere between 513 and 673 K,[70] dependent on the degree of hydration. The TPS profiles for the sulfidation of the MoO_3/SiO_2 catalysts roughly correspond to those found by Arnoldy[86] for MoO_3/Al_2O_3 catalysts.

The exact structure transformations under sulfiding conditions have been investigated for catalyst Mo6 that possesses a well established structure in the oxidic state. The structure of the oxidic *precursor* of the sulfided phase can be described as an oligomeric cluster, comparable to the hepta/octamolybdate units in aqueous solution.[87–88] Under sulfiding conditions (H_2S/H_2/Ar) at room temperature the cluster disrupts. About half of the oxygen atoms in the cluster disappear by *oxygen–sulfur exchange*. According to the EXAFS data, only a small fraction of the oxygen atoms remain, which probably represent terminal Mo=O bonds,

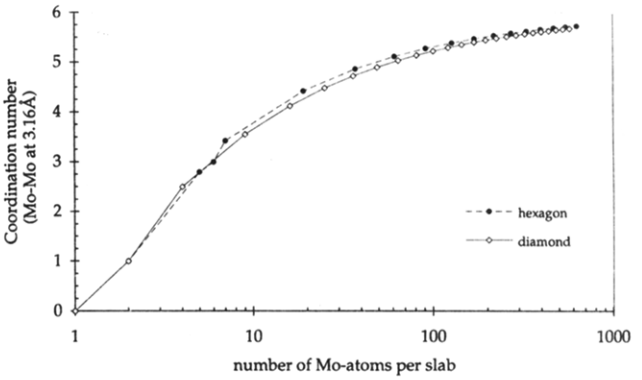

Figure 11. $N^{\text{model}}_{\text{Mo—Mo}}$ as a function of the model slab size (diamond or hexagon shaped).

Figure 12. TEM micrograph of Mo6-673. The distance between the two short arrows amounts to about 12 Å (twice the length of the *c*-axis in MoS_2 (6.16 Å), or the "interslab distance").

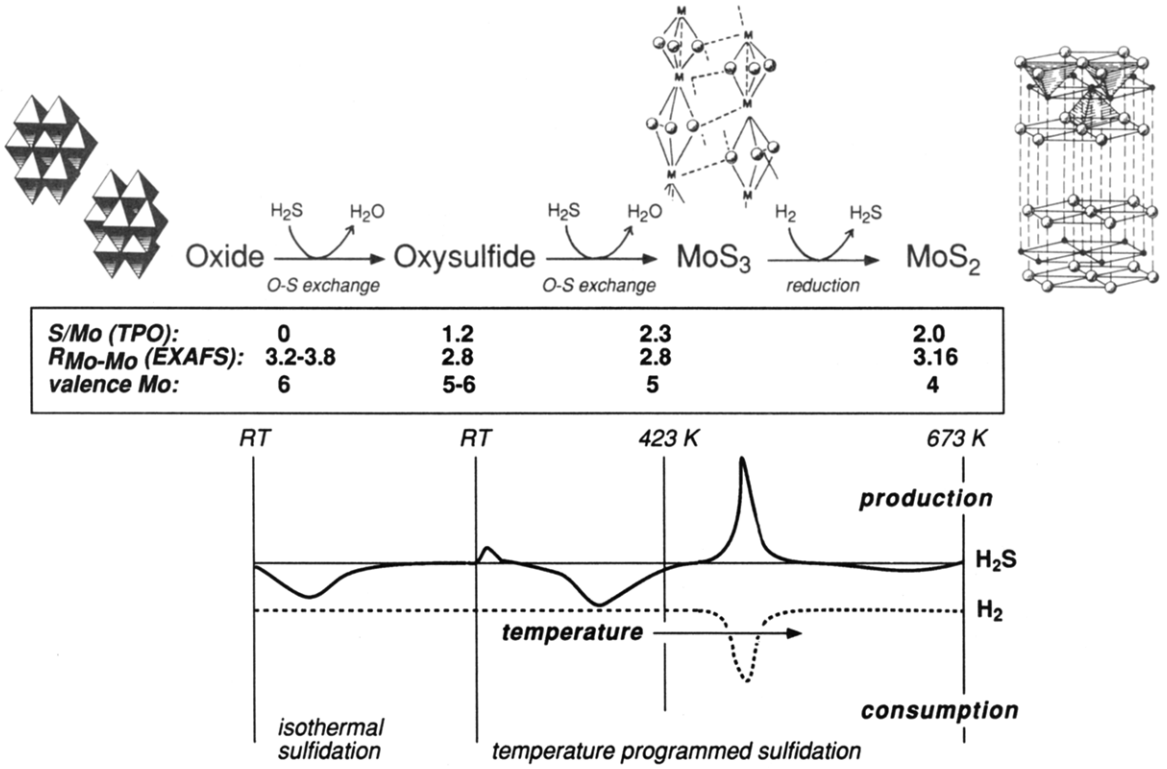

Figure 13. Synopsis of the sulfidation mechanism of well-dispersed SiO_2-supported MoO_3 clusters. Evolution of the oxidic oligomeric cluster via oxysulfide and MoS_3 into the final MoS_2 slabs.

because of the small $R_{Mo=O}$ (high bond strength). According to TPO, the S/Mo ratio in Mo6-RT amounts to 1.4, indicating a lower degree of sulfidation than suggested by EXAFS analysis of the first shell. These observations are reasonably in agreement with earlier reported sulfidation studies. Most authors mention the take-up of H_2S at room temperature for SiO_2- or Al_2O_3-supported (Co)Mo catalysts.[47,48] Few of them, however, report on deep sulfidation at room temperature.

The clusters assume a structure comparable to that of MoS_3, as shown by the characteristic, short R_{Mo-Mo} of 2.755 Å. A value of about 2.8 Å for the Mo—Mo bond length is mentioned by Goodenough[84] and Liang[85] and strongly diverges from the R_{Mo-Mo} in MoS_2 (3.16 Å). The brownish color of Mo6-RT and Mo6-423 confirms the presence of MoS_3-like clusters.[26,27] The existence of MoS_3 during sulfidation of MoO_3 catalysts has been reported in the literature but has not been shown by means of EXAFS before. From the absence of a pre-edge peak in Mo6-RT, Mo6-423, and Mo6-673, it must be concluded that no tetrahedrally coordinated molybdenum and, therefore, no hexavalent molybdenum can be present. The exchange of oxygen for sulfur anions in Mo6, occurring during sulfidation at room temperature, simultaneously reduces the molybdenum to 5+. This implies that S_2^{2-} (persulfide) anions are present, as in MoS_3. Experimental verification of the existence of Mo^{5+} and S_2^{2-} should be done by means of XPS.

Sulfidation at higher temperatures (Mo6-423) gives rise to the exchange of the last oxygen, and even to a S/Mo value higher than 2 in TPO. EXAFS analysis on Mo6-423 does not reveal a Mo—O contribution anymore, and a high Mo—S coordination number is found. The sulfided molybdenum clusters in Mo6-423 have a surplus of sulfur sites (S/Mo > 2) that possess a high reactivity. The instability of the MoS_3-like structure in Mo6-423 leads to release of H_2S at approximately 553 K with consumption of H_2. The eventually formed cluster has the structure of MoS_2, as shown by the R_{Mo-S} value of 2.41 Å and the R_{Mo-Mo} value of 3.16 Å. The N_{Mo-S} value of 6.00 perfectly matches the 6-coordination in MoS_2. This is in agreement with the black color of the sample. The two-dimensional slab size can be estimated from N_{Mo-Mo} by a simple model. The slab size amounts to approximately 34 molybdenum atoms, according to this model. The mean stack height, derived from TEM, is about 3. The large number of molybdenum atoms per MoS_2 particle is caused by sintering due to the loss of interaction of the MoS_2 slabs with the SiO_2 support and the exothermicity of the reduction at 553 K.[70] Both factors lead to the coalescence of the particles.

A synopsis of the reactions taking place during the sulfidation of well-defined SiO_2-supported MoO_3 clusters in H_2S/H_2 is given in Figure 13. The figure indicates the evolution from an oxidic cluster (like heptamolybdate) via a partially sulfided cluster (oxysulfide) to a MoS_3-like cluster, that is eventually reduced to an MoS_2 slab. The corresponding properties (S/Mo, R_{Mo-Mo}, valence) characteristic of the cluster during the sulfidation are represented and correspond well to the features in the TPS experiment.

Acknowledgment. We gratefully acknowledge the financial support of Akzo Nobel Chemicals B.V. (Amsterdam, The Netherlands).

References and Notes

(1) Haber, J. *Proc. 8th ICC*; Berlin, 1984; vol. 1, p 85.
(2) Iwasawa, Y.; Nakamura, T.; Takamatsu, K.; Ogasawara, S. *J. Chem. Soc., Faraday Trans 1* **1980**, *76*, 939.
(3) Cullis, C. F.; Hücknall, D. J. *Catalysis* **1982**, *5*, 273.
(4) Dadyburjor, D. B.; Jewur, S. S.; Rückenstein, E. *Catal. Rev.-Sci. Eng.* **1979**, *19(2)*, 293.
(5) Knözinger, H. *Proc. 9th ICC (Calgary)* **1988**, *1*, 20.
(6) Prins, R.; de Beer, V. H. J.; Somorjai, G. A. *Catal. Rev.-Sci. Eng.* **1989**, *31*, 1.
(7) Topsøe, H.; Clausen, B. S. *Appl. Catal.* **1986**, *25*, 273.
(8) Topsøe, H.; Clausen, B. S.; Topsøe, N. Y.; Pedersen, E. *Ind. Eng. Chem. Fundam.* **1986**, *25*, 25.
(9) Topsøe, H.; Clausen, B. S. *Catal. Rev.-Sci. Eng.* **1984**, *26(3&4)*, 395.
(10) Zdrazil, M. *Bull. Soc. Chim. Belg.* **1991**, *100*, 769.
(11) Luck, F. *Bull. Soc. Chim. Belg.* **1991**, *100*, 781.
(12) Aalund, L. R. *Oil Gas J.* **1984**, *82(41)*, 55.
(13) Moyes, R. B. *Chem. Ind.* **1988**, *31*, 583.
(14) Ohtsuka, T. *Catal. Rev.-Sci. Eng.* **1977**, *16(2)*, 291.
(15) Grange, P. *Catal. Rev.-Sci. Eng.* **1980**, *21(1)*, 135.
(16) Chianelli, R. R. *Catal. Rev.-Sci. Eng.* **1984**, *26(3&4)*, 361.
(17) Friend, C. M.; Roberts, J. T. *Acc. Cem. Res.* **1988**, *21*, 394.
(18) Grange, P.; Delmon, B. *J. Less-Common Met.* **1974**, *36*, 353.
(19) Hallie, H. *Oil Gas J.* **1982**, *80(51)*, 69.

(20) Prada Silvy, R.; Grange, P.; Delannay, F.; Delmon, B. *Appl. Catal.* **1989**, *46*, 113.
(21) Berrebi, G.; Roumieu, R. *Bull. Soc. Chim. Belg.* **1987**, *96*, 967.
(22) Topsøe, H. *J. Catal.* **1983**, *84*, 386.
(23) Arteaga, A.; Fierro, J. L.; Delannay, F.; Delmon, B. *Appl. Catal.* **1986**, *26*, 227.
(24) Fleischauer, P. D.; Lince, J. R.; Bertrand, P. A.; Bauer, R. *Langmuir* **1989**, *5*, 1009.
(25) Bertrand, P. A. *Langmuir* **1989**, *5*, 1387.
(26) Payen, E.; Kasztelan, S.; Houssenbay, S.; Szymanski, R.; Grimblot, J. *J. Phys. Chem.* **1989**, *93*, 6501.
(27) Pratt, K. C.; Sanders, J. V.; Christov, V. *J. Catal.* **1990**, *124*, 416.
(28) Günter, J. G.; Marks, O.; Korányi, T. I.; Paál, Z. *Appl. Catal.* **1988**, *39*, 285.
(29) Cruz-Reyes, J.; Avalos-Borja, M.; Farías, M. H.; Díaz, G.; Fuentes, S. *Mater. Lett.* **1989**, *8(11/12)*, 492.
(30) Topsøe, H.; Clausen, B. S.; Candia, R.; Wivel, C.; Mørup, S. *J. Catal.* **1981**, *68*, 433.
(31) Eijsbouts, S.; Heinerman, J. J. L.; Elzerman, H. J. W. *Appl. Catal. A* **1993**, *105*, 53; **1993**, *105*, 69.
(32) Eijsbouts, S.; Heinerman, J. J. L.; Elzerman, H. J. W. Akzo Catalysts Symposium 1991, Hydroprocessing; Scheveningen, 1991; p 201.
(33) Parham, T. G.; Merrill, R. P. *J. Catal.* **1984**, *85*, 295.
(34) Gates, B. C.; Katzer, J. R.; Schuit, G. C. A. *Chemistry in Catalytic Processes*; McGraw-Hill: New York, 1979; p 411.
(35) Farragher, A. L.; Cossee, P. In *Proc. 5th ICC* (Palm Beach, 1972); Hightower, J. W., Ed.; Amsterdam, 1973; p 1301.
(36) Voorhoeve, R. J. H.; Stuiver, J. C. M. *J. Catal.* **1971**, *23*, 243.
(37) Pirotte, D.; Zabala, J. M.; Grange, P.; Delmon, B. *Bull. Soc. Chim. Belg.* **1981**, *90*, 1239.
(38) Wivel, C.; Candia, R.; Clausen, B. S.; Topsøe, H. *J. Catal.* **1981**, *68*, 453.
(39) Ratnasamy, P.; Sivasanker, S. *Catal. Rev.-Sci. Eng.* **1980**, *22*, 401.
(40) van Veen, J. A. R.; Gerkema, E.; van der Kraan, A. M.; Hendriks, P. A. J. M.; Beens, H. *J. Catal.* **1992**, *133*, 112.
(41) van der Kraan, A. M.; Crajé, M. W. J.; Gerkema, E.; Ramselaar, W. L. T. M.; de Beer, V. H. J. *Appl. Catal.* **1988**, *39*, L7.
(42) Crajé, M. W. J. Ph.D. Thesis, Delft, 1992 (ISBN 90-73861-08-X).
(43) de Beer, V. H. J.; Duchet, J. C.; Prins, R. *J. Catal.* **1981**, *72*, 369.
(44) Duchet, J. C.; van Oers, E. M.; de Beer, V. H. J.; Prins, R. *J. Catal.* **1983**, *80*, 386.
(45) Crajé, M. W. J.; de Beer, V. H. J.; van der Kraan, A. M. *Bull. Soc. Chim. Belg.* **1991**, *100*, 953.
(46) Crajé, M. W. J.; de Beer, V. H. J.; van der Kraan, A. M. *Appl. Catal.* **1991**, *70*, L7.
(47) Arnoldy, P. Ph.D. Thesis, Amsterdam, 1985.
(48) Mangnus, P. J. Ph.D. Thesis, Amsterdam, 1991.
(49) Scheffer, B.; Dekker, N. J. J.; Mangnus, P. J.; Moulijn, J. A. *J. Catal.* **1990**, *121*, 31.
(50) Scheffer, B.; Mangnus, P. J.; Moulijn, J. A. *J. Catal.* **1990**, *121*, 18.
(51) Schrader, G. L.; Cheng, C. P. *J. Catal.* **1983**, *80*, 369.
(52) Candia, R.; Clausen, B. S.; Topsøe, H. *Bull. Soc. Chim. Belg.* **1981**, *90(12)*, 1225.
(53) Bouwens, S. M. A.; Prins, R.; de Beer, V. H. J.; Koningsberger, D. C. *J. Phys. Chem.* **1990**, *94*, 3711.
(54) Bouwens, S. M. A.; Koningsberger, D. C.; de Beer, V. H. J.; Louwers, S. P. A.; Prins, R. *Catal. Lett.* **1990**, *5*, 273.
(55) Clausen, B. S.; Lengeler, B.; Candia, R. *Bull. Soc. Chim. Belg.* **1981**, *90(12)*, 1249.
(56) Clausen, B. S.; Lengeler, B.; Topsøe, H. *Polyhedron* **1986**, *5*, 199.
(57) Sankar, G.; Vasudevan, S.; Rao, C. N. *J. Phys. Chem.* **1987**, *91*, 2011.
(58) Boudart, M.; Dalla Betta, R. A.; Foger, K.; Löffler, D. G.; Samant, M. G. *Science* **1985**, *228*, 717.
(59) Chiu, N.-S.; Bauer, S. H.; Johnson, M. F. L. *J. Catal.* **1984**, *89*, 226.
(60) Chiu, N.-S.; Bauer, S. H.; Johnson, M. F. L. *J. Catal.* **1986**, *98*, 32.
(61) Grove, C. L.; Schmidt, L. D. *Appl. Surf. Sci.* **1988–89**, *35*, 199.
(62) Delannay, F. *Appl. Catal.* **1985**, *16*, 135.
(63) Villa-Garcia, M. A.; Lindner, J.; Sachdev, A.; Schwank, J. *J. Catal.* **1989**, *119*, 388.
(64) Korányi, T.; Manninger, I.; Paál, Z.; Marks, O.; Günter, J. R. *J. Catal.* **1989**, *116*, 422.
(65) Sanders, J. V. *Chem. Scripta.* **1978**, *14*, 141.
(66) Prasad, V.; Chary, K.; Rao, K. S.; Rao, P. K. *J. Chem. Soc., Chem. Commun.* **1989**, 1746.
(67) Chary, K. V. R.; Rao, P. K.; Prasad, V. V. D. N.; Rao, K. S. *J. Mol. Catal.* **1990**, *63*, L21.
(68) Cruz-Reyes, J.; Avalos-Borja, M.; Farías, M. H. *Catal. Lett.* **1989**, *3*, 227.
(69) Fuentes, S.; Diaz, G.; Pedraza, F.; Rojas, H.; Rosas, N. *J. Catal.* **1988**, *113*, 535.
(70) Weisser, O.; Landa, S. *Sulfide Catalysts, Their Properties and Applications*; Pergamon Press: Oxford-New York, 1973; pp 39, 44.
(71) Müller, A.; Diemann, E.; Branding, A.; Baumann, F. W.; Breysse, M.; Vrinat, M. *Appl. Catal.* **1990**, *62*, L13.
(72) Arnoldy, P.; Moulijn, J. A. *J. Catal.* **1985**, *93*, 38.
(73) de Roos, G.; Fluit, J. M.; de Wit, J. H. W.; Geus, J. W. *Surf. Interface Anal.* **1981**, *3*, 229.
(74) Carvill, B. T.; Thompson, L. T. *Appl. Catal.* **1991**, *75*, 249.
(75) Potoczna-Petru, D.; Kepínski, L. *Catal. Lett.* **1991**, *9*, 355.
(76) (a) de Boer, M.; van Dillen, A. J.; Koningsberger, D. C.; Geus, J. W.; Vuurman, M. A.; Wachs, I. E. *Catal. Lett.* **1991**, *227*. (b) de Boer, M. Ph.D. Thesis, University of Utrecht, 1992 (ISBN 90-393-0384-3).
(77) Stuchly, V.; Zahradnikova, H.; Beranek, L. *Appl. Catal.* **1987**, *35*, 23.
(78) Wittneben, V.; Sprafke, A.; Diemann, E.; Müller, A.; Kuetgens, M.; Chauvistre, R.; Hormes, J. *J. Mol. Struct.* **1989**, *198*, 525.
(79) Bhattacharya, R. N.; Lee, C. Y.; Pollak, F. H.; Schleich, D. M. *J. Noncryst. Solids* **1987**, *91*, 235.
(80) Schleich, D. M.; Chang, H. S.; Barberio, Y. L.; Hanson, K. J. *J. Electrochem. Soc.* **1989**, *136(11)*, 3274.
(81) Chang, C. H.; Chan, S. S. *J. Catal.* **1981**, *72*, 139.
(82) Yoshimura, Y.; Sato, T.; Shimada, H.; Matsubayashi, N.; Nishjima, A. *Appl. Catal.* **1991**, *73*, 55.
(83) van Doorn, J.; Barbolina, H. A. A.; Moulijn, J. A. *Ind. Eng. Chem. Res.* **1992**, *31*, 101.
(84) Goodenough, J. B. In *Proc. 4th Int. Conf. Chem. Uses Molybdenum*; Barry, H. F., et al., Ed.; Climax Molybdenum Co.: Ann Arbor, MI, 1984; p 1.
(85) Liang, K. S.; de Neufville, J. P.; Jacobson, A. J.; Chianelli, R. R.; Betts, F. *J. Noncryst. Solids* **1980**, *35/36(II)*, 1249.
(86) Arnoldy, P.; van den Heijkant, J. A. M.; de Bok, G. D.; Moulijn, J. A. *J. Catal.* **1985**, *92*, 35.
(87) Kepert, D. L. In *Comprehensive Inorg. Chem.*, part 4; Bailar, J. C., Ed.; Pergamon Press: Oxford, p 607.
(88) Baes, C. F.; Mesmer, R. E. *The Hydrolysis of Cations*; J. Wiley & Sons: New York, 1976.
(89) Prins, R. Private communication.
(90) Kampers, F. W. H.; Maas, T. M. J.; van Grondelle, J.; Brinkgreve, P.; Koningsberger, D. C. *Rev. Sci. Instrum.* **1989**, *60*, 2635.
(91) Van Zon, J. B. A. D.; Koningsberger, D. C.; Van't Blik, H. F. J.; Sayers, D. E. *J. Chem. Phys.* **1985**, *82*, 5742.
(92) Bouwens, S. M. A.; Prins, R.; de Beer, V. H. J.; Koningsberger, D. C. *J. Phys. Chem.* **1990**, *94*, 3711.
(93) de Boer, M.; van Dillen, A. J.; Koningsberger, D. C.; Geus, J. W. *Jpn. J. Appl. Phys.* **1993**, 460.
(94) de Boer, M.; Leliveld, R. G.; van Dillen, A. J.; Geus, J. W.; Bruil, H. G. *Appl. Catal.* **1993**, *102*.